FR 8602064

COMMISSARIAT A L'ENERGIE ATOMIQUE

CENTRE D'ETUDES NUCLEAIRES DE SACLAY
Service de Documentation
F91191 GIF SUR YVETTE CEDEX

CEA-CONF - - 8255

L5

THERMAL TRANSPORT EXPERIMENTS AT 0.35 µm LASER WAVELENGTH

D. Juraszek, M. Bernard, D. Billon, J.L. Bocher, P.A. Holstein, J.P. Le Breton, M. Louis-Jacquet, D. Meynial, and Ph. Schneider

Commissariat à l'Energie Atomique
Centre d'Etudes de Limeil-Valenton
B.P. n° 27, 94190 Villeneuve-Saint-Georges, France

Communication présentée à : 7. International workshop on laser interaction and related plasma phenomena
Monterey, CA (USA)
28 Oct - 1 Nov 1985

THERMAL TRANSPORT EXPERIMENTS AT 0.35 μm LASER WAVELENGTH

D. Juraszek, M. Bernard, D. Billon, J.L. Bocher,
P.A. Holstein, J.P. Le Breton, M. Louis-Jacquet,
D. Meynial, and Ph. Schneider

Commissariat à l'Energie Atomique
Centre d'Etudes de Limeil-Valenton
B.P. n°. 27, 94190 Villeneuve-Saint-Georges, France

ABSTRACT

Layered plane targets have been irradiated with 0.35 μm laser wavelength at the power level 0.1 TW using the Nd-glass laser system Octal equipped with KDP tripling systems. Four beams were superimposed on a 150 μm in diameter focal spot. Propagation of the thermal front ($T > 10^6$K) was analysed by means of time-resolved recording of the sub-keV X-ray target emission. A comparison to computer simulations shows that the results can be described by a flux limiter $f = 0.03 \pm 0.015$.

INTRODUCTION

Many laser-matter interaction experiments have been devoted to the study of energy transport from the laser deposition region to the dense region of the target [1]. First because the plasma of interest sensitively depends on this transport. For example in the case of direct drive implosions it determines the hydrodynamic efficiency [2] ; it also has an effect on the way the laser is absorbed and on the conversion of this absorbed energy into X-rays [3]. On the other hand the so-called transport experiments are necessary because there is not any theoritical model describing the whole phenomenon for the time being. Moreover the energy can be transported by thermal electrons, suprathermal electrons and X-rays. In the following we are going to focus on the first term only, unless otherwise stated.

Indeed Gray and Kilkenny [4] pointed out that Spitzer-Harm theory is no longer valid for the collisionnality λ_0/LT larger than 2×10^{-3} (λ_0 is the mean free paths for 90° scattering, LT is the scale length of the temperature gradient). Now in the cases that we are going to deal with, this ratio can reach 10^{-1}.

In the hydrocodes used to interpret the experiment the heat flux q, is function of Spitzer-Harm flux and of the free-streaming flux :

$$\vec{q}_{SH} = -K_o T^{5/2} \vec{\nabla} T$$

$$\vec{q}_{FS} = 0.64\, n_e\, KT_e\, v_T \frac{\vec{\nabla} T}{|\vec{\nabla} T|}$$

let be either

$$q = \min (q_{SH}, Fq_{FS}) \qquad (1)$$

or

$$\vec{q} = \frac{q_{SH}\, Fq_{FS}}{q_{SH} + Fq_{FS}} \frac{\vec{\nabla} T}{|\vec{\nabla} T|} \qquad (1')$$

Where F is an adjustable parameter ; f = 0.64 F is called "flux limiter" in the litterature.

The obtained values of f vary from experiment to experiment very much, particularly with the laser wavelength λ_L, the target geometry, the flux, ...

Recently codes based on Fokker-Planck equation solution brougth some new results [6] :

- it is not necessary to invoke anomalous phenomena (magnetic field, ion acoustic turbulence ...) to explain f = 0.1 in the case of λ_L = 0,35 μm ;
- for $_o$/LT in the range 10^{-2} - 10^{-1} the transport is delocalized and cannot be described by (1) or (1'). This effect contributes to modify the temperature profile.

In this paper we want to describe an experiment using two improvements into the multilayer target technique [8 9] :

- the time resolution : it has been used at RAL in order to observe the characteristic lines of Al and Si. This method is only sensitive to temperatures larger than 300 eV. It has been used at LLE in order to observe the continuous X rays for hν larger than 1 keV ;

- the observation of X rays in the range 200 - 1000 eV : it enables us to measure temperature about 100 eV. This method has been used by Mead et al [12], X rays being recorded by X-ray diodes (XRD).

The observation of subkeV X rays with time resolution has been proposed by G.L. Stradling [13]. But this experiment did not give any "burn through" [12 13].

We made an experiment similar to the previous one. The results that we obtained are compared to numerical lagragian simulation using the relation (1') to calculate the heat flux.

EXPERIMENTAL CONDITIONS

Laser and irradiation

For these experiments we used four beams from the Octal Nd glass laser system. The IR light is converted into 0.35 μm by type II KDP crystals. The f/5 lens axes are on a 22°5 half angle cone (Fig. 1a). The focal spots were superimposed to reduce irradiation non-uniformities ; Fig. 2a shows a near field converted beam profile. The resulting illumination deduced from pinhole camera measurements (Fig. 2b) with a 10 μm resolution can be fitted by :

$$E(r) = E_0 \exp\left(-\ln 2 (r/\Delta r_{1/2})^4\right) \qquad (2)$$

For the experiments $2r_{1/2}$ = 150 μm. The incident laser energy was about 100 J. The pulse shape had a full width at half maximum of approximately 1 ns, with a fast rise time : 200 ps between 0.1 P_{max} and 0.9 P_{max}. In these conditions, the irradiance was about $(6+2)10^{14}\ W/cm^2$. TFF1 Hoya filters and the chromatic shift of the lenses reduced the 1.06 and 0.53 μm on target fluxes to 10^{-5} and 4 10^{-6} of the 0.35 μm flux.

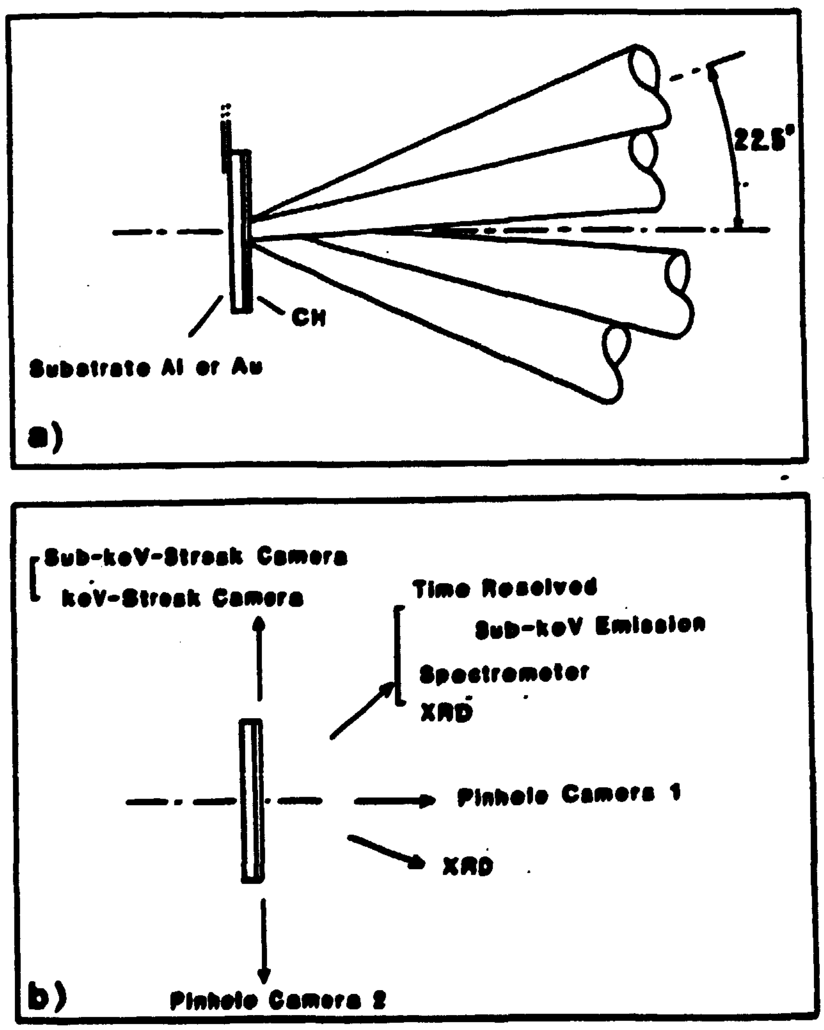

Fig. 1. Experimental apparatus

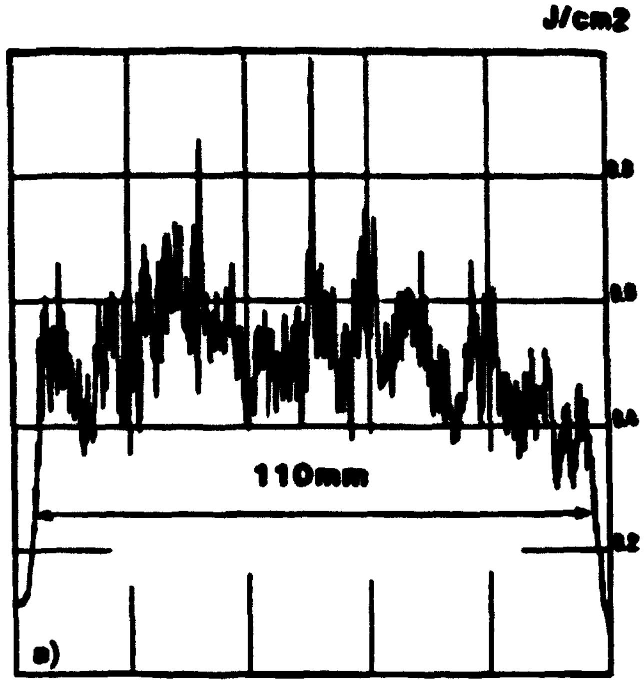

Fig. 2a. Near field converted beam profile

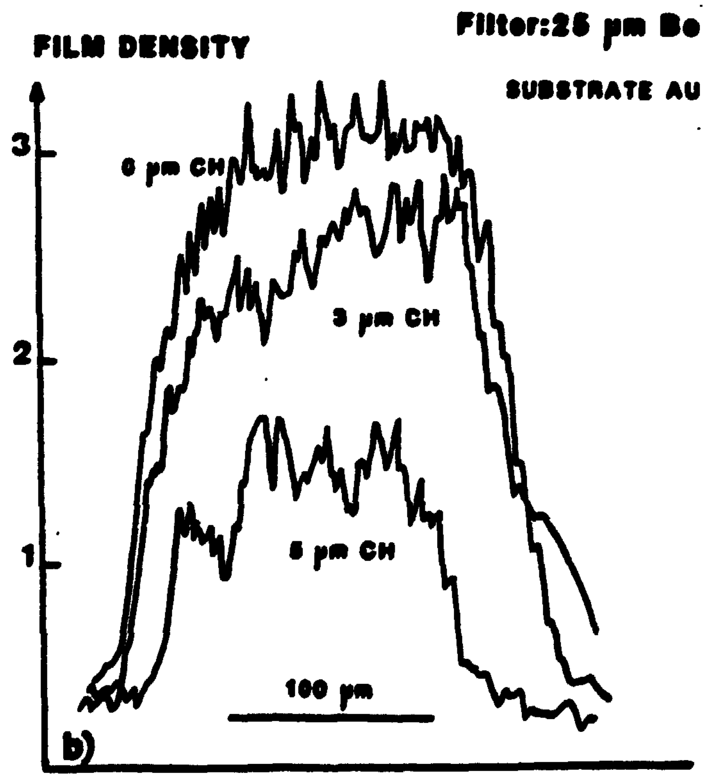

Fig. 2b. X-ray pinhole camera images at 0° to the cluster axis

Targets

The targets were gold or aluminum disk 1000 μm in diameter and 20μm thick coated with polystyrene. The coating thickness ranged from 0 μm to 10 μm, its density was (1.4 ± 0.1) g/cm^3 and its thickness was measured to within ± 0.05 μm.

For most shots the target was normal to the beams cluster axis (Fig.1).

Diagnostics description and location

Fig. 1b gives the main diagnostics position. The absorbed energy was measured by an array of glass absorbing calorimeters or by plasma calorimeters. Two pinhole cameras viewing the target at 0° and 90° provided plasma images in the keV range with a 10 μm spatial resolution.

Two K-edge filtered X-ray diode detector systems, (XRD) at 22°5 and 55° to the cluster axis, gave the continuum emission spectra from 200 eV to 30 keV and an estimation of the total radiated X-ray energy.

A TlAP crystal spectrograph recorded the aluminum spectrum in the 5-8 Å range.

X-ray streak cameras gave space or spectral-time resolved informations. Two space resolved cameras viewed the target at 90° from cluster axis. The first one covered the kiloelectronvolt range (about 1.5 keV to 10 keV) ; the spatial resolution was obtained with a simple slit. The second system observed the subkiloelectronvolt emission ($h\nu \simeq 200$ - 2000 eV) and it was equipped with a P 650 camera [14] ; the spatial resolution was realized with a toroidal grazing incidence (2°) gold mirror, which transmits only low energy radiation (h < 2 keV).

The main diagnostic of these series of experiments was the time resolution of the sub-keV X-ray emission. It associated a P 550 camera[15] with a 300 Å gold photocathode deposited on a 1 μm thick polystyrene substrate and an array of K and L edge filters (Fig. 3a) ; Fig. 3b gives the photocathode sensivity. The grazing incidence glass mirror cuts radiations above 500 eV, only the CH channel was used with mirror. For the other channels the energy above the K or L edge was eliminated by an iterative calculation. Fig. 3c gives the different channels response to a characteristic spectrum (the high energy responses are omitted).

No time fiducial was avalaible with this device. The intrinsic time resolution of the camera was about 20 ps.

EXPERIMENTAL RESULTS AND NUMERICAL SIMULATIONS

Numerical simulations models

With the lagrangian code FCI1 we have performed one dimensional plane and spherical simulations. For the spherical cases the curvature radius was 2.5 times the focal spot diameter. To account for the beams incidence, the laser wavelength was $(0.35 \cos^{-1} (22.5))$ μm. The laser energy was absorbed by inverse bremsstrahlung, only a small fraction being dumped at critical density. We hava neglected the effects of suprathermal electrons generated by resonance absorption or by 2 ωp and Raman instabilities [12 16 18].

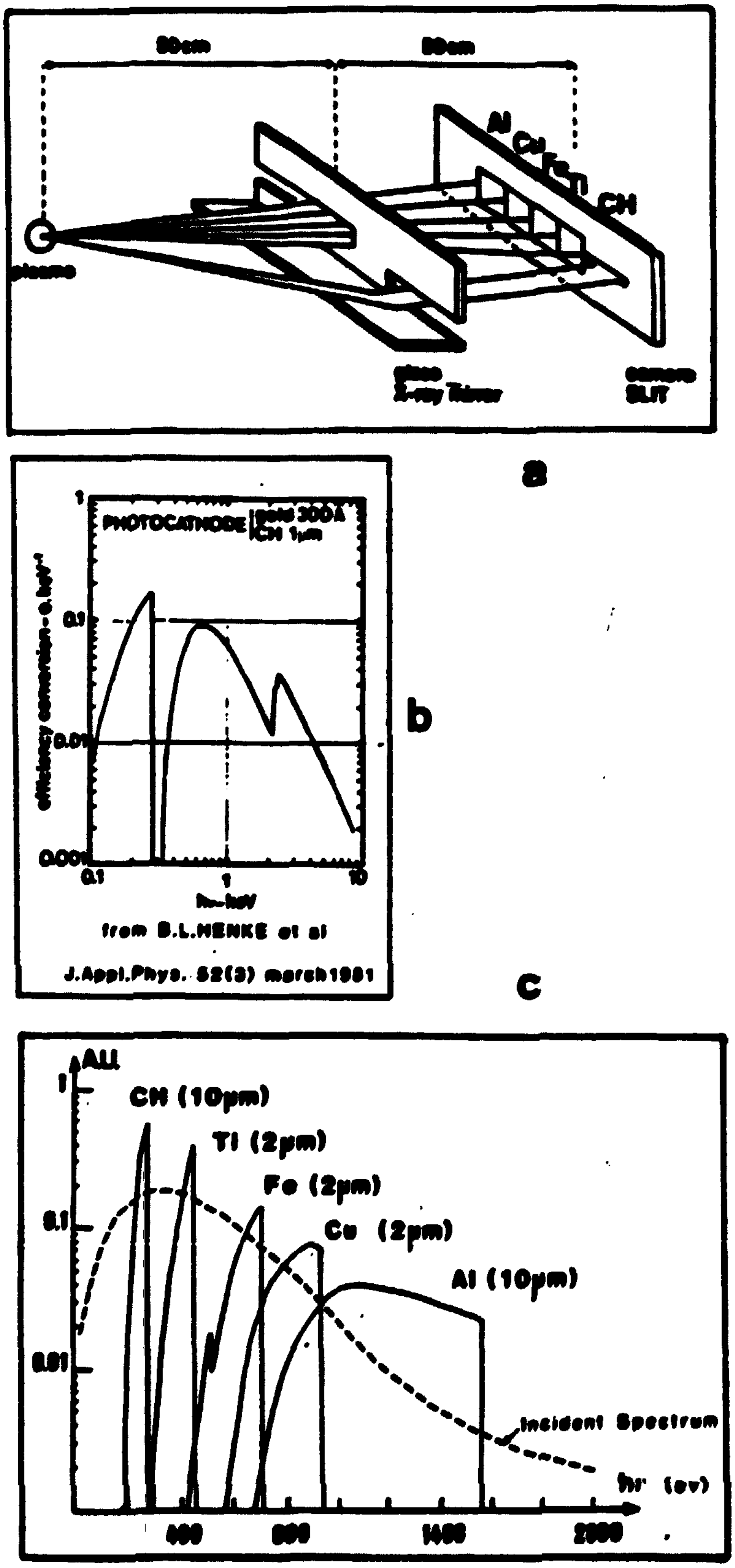

Fig. 3 a) Schematic of soft X-ray streak system
b) Photocathode sensitivity
c) Channel responses to a characteristic spectrum

In the code, the thermal electrons flux, is calculated with relation (1) ; the X-ray energy transport is treated by a multigroup diffusion method, with variable Eddington factor. The Al and CH emission lines are not included.

Calculations with Au substate used a non-local-thermodynamic equilibrium (non LTE) treatment based on the mixed model made by M.Busquet[19].

The results obtained with the one dimensional code were compared to 2D calculations with the FCI2 lagrangian code. In these simulations the magnetic field was not included and the flux limiter was independent of the direction.

Experimental results interpretation

Absorption efficiency. Absorption efficiency measurements can provide a first indirect information on thermal transport. In our experimental conditions (laser wavelength and irradiation), inverse bremsstrahlung is believed to be the dominant absorption mechanism. But this process depends on the plasma electron temperature : $K_{abs} \sim T_e^{-3/2}$ [20] and the corona temperature is a function of the flux limiter [2].

On the figure 4 we compare the numerical results to the experiment. For one dimensional simulations the best agreement is obtained for f between 0.03 and 0.06. This result is similar to those obtained at LLE [21] [22].

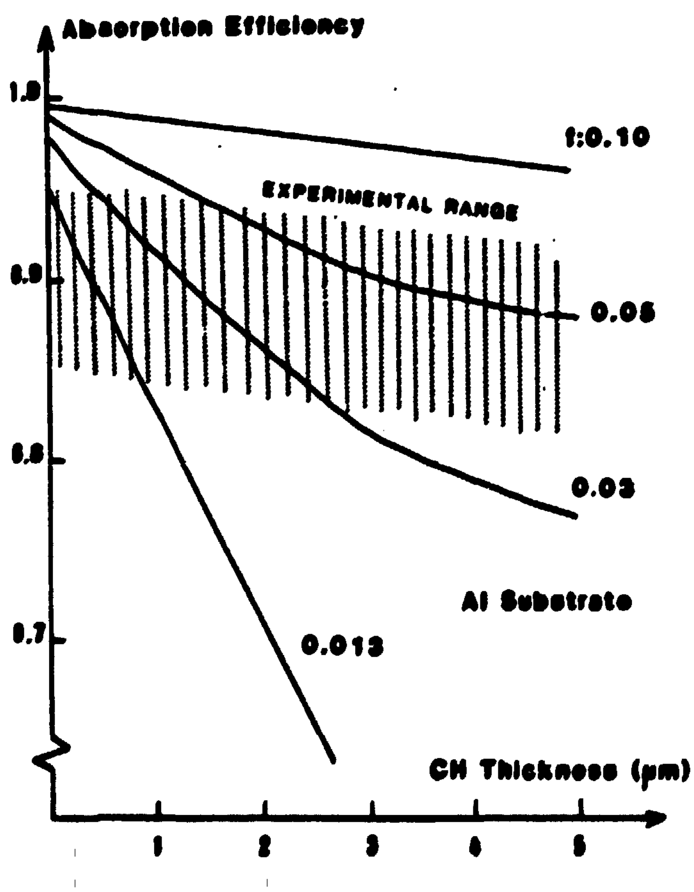

Fig. 4. Measured and calculated absorption efficiency (Aluminum substrate)

We have to notice that for aluminum the calculated absorption is overestimated. This can be explained by the LTE ionisation model we have used.

2D calculations predict a somewhat higher absorption rate for the same flux limiter value, but no systematic comparison was made.

<u>Time resolved subkiloelectronvolt X-ray emission</u>. On figure 5 we give typical results obtained with 3 μm CH coated target and the two kinds of substrate. We can observe that in each cases the burnthrough signal is well defined. That means we have a rather uniform irradiation and that non local transport is non significant.

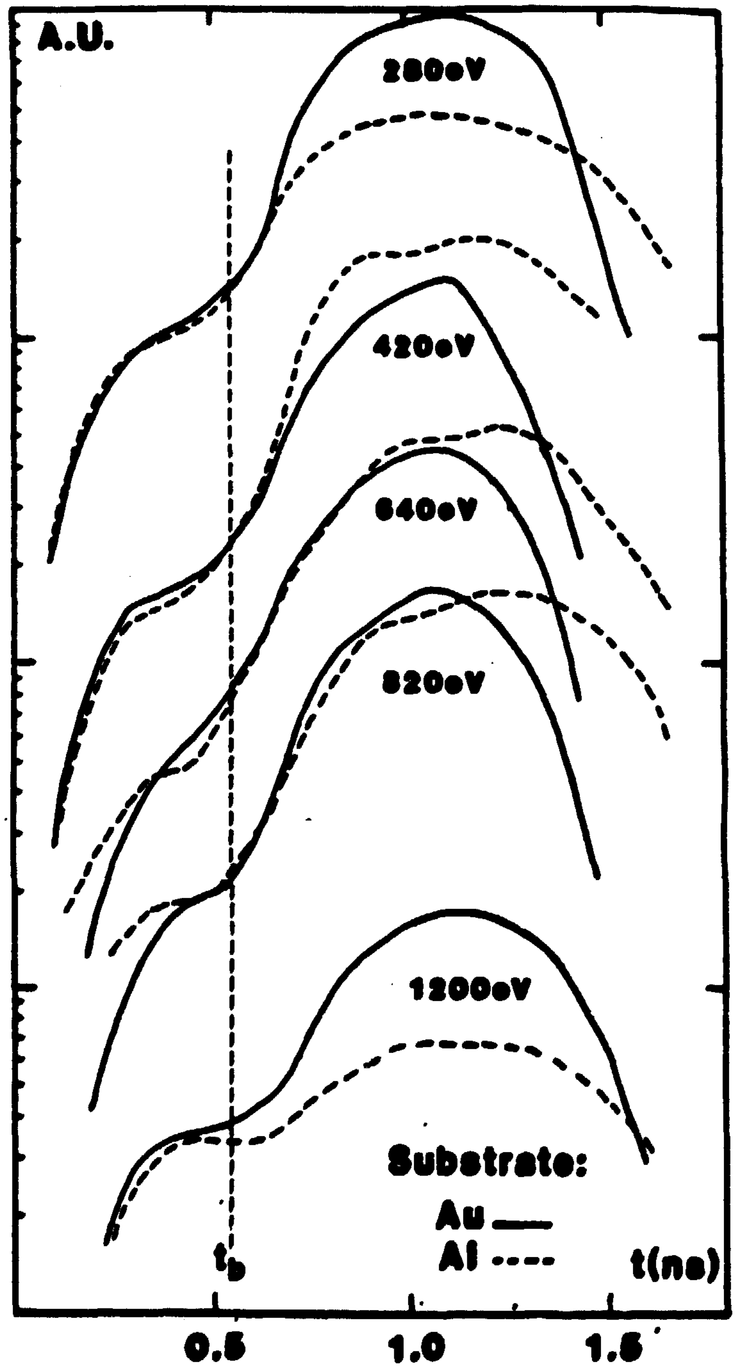

Fig. 5. Measured X-ray emission time histories ($h\nu$ < 1.5 keV) for a 3 μm CH coating thickness, for sake of clarity results of different channels have been arbitrary translated along the X-ray intensity axis

We can also notice that the measured burnthrough time does not depend on substrate material. The difference between Al and Au appears in the maximum signal amplitude and especially in the signal decrease : Al emission decreases more slowly than the laser pulse and than Au emission.

The last interesting feature is that the burnthrough time is approximately the same for all channels, except for the 1200 eV channel. This result can be explain by a rather steep thermal front and as pointed out previously by negligible non local effects.

The lower energy channels are used to define the burnthrough time t_B.

Because the camera was not absolutely calibrated, we have compared the signal shapes but not their levels. The use of 1D simulations supposes that lateral transport is negligible ; we shall come back on this point later.

The figures 6, 7 and 8 give examples of numerical restitutions, with 1, 3 or 5 μm CH coating on aluminum targets ; the best over-all agreement was obtained for f : 0.03 ± 0.015.

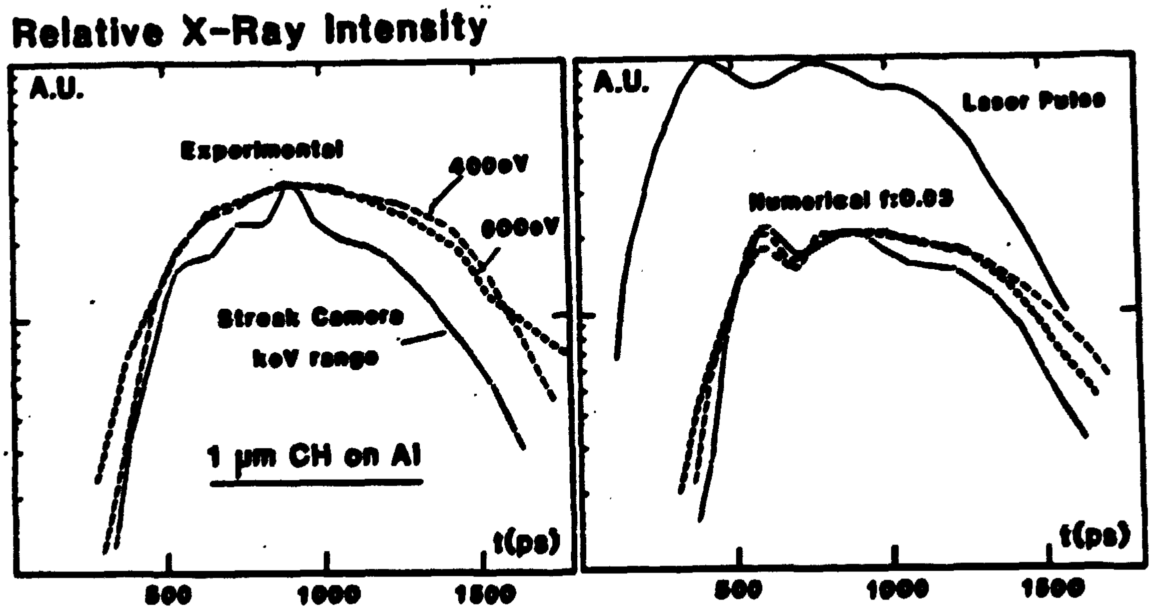

Fig. 6. Calculated and measured X-ray emission time histories ; 1 μm CH coating thickness on aluminum ; the different curves have been normalized to the same maximum value

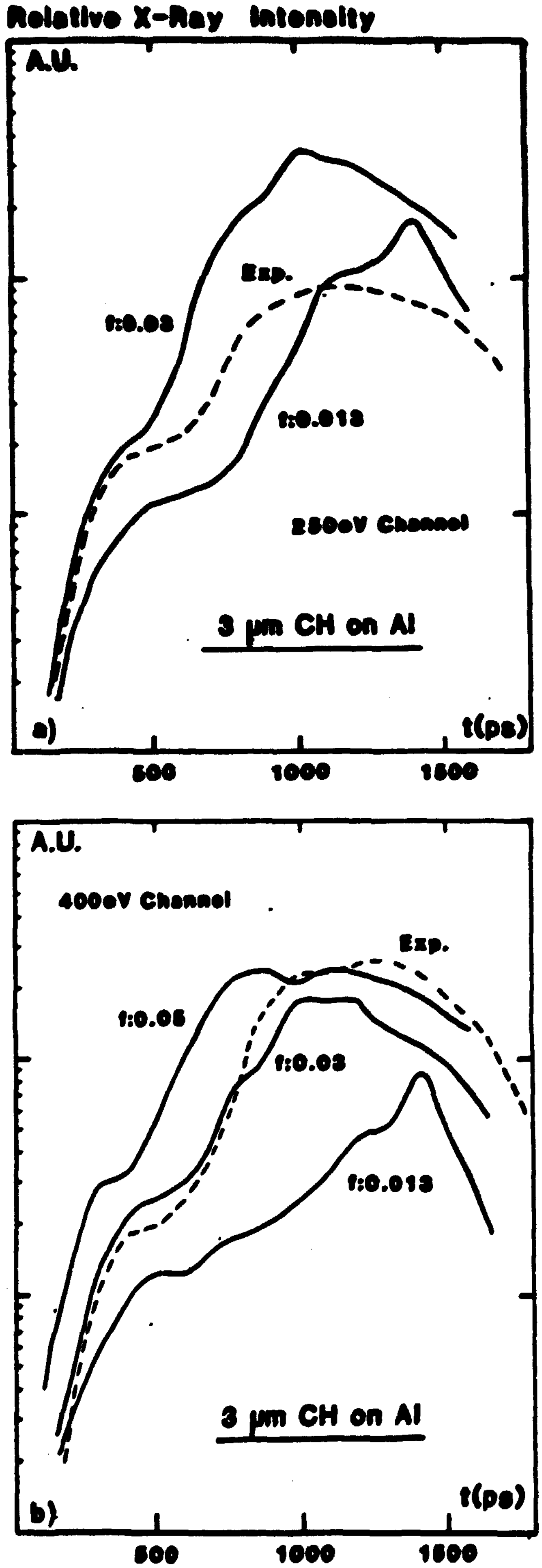

Fig. 7. Calculated and measured X-ray emission time histories ;
3 μm CH coating thickness on aluminum.
a) hν ≃ 250 eV b) hν ≃ 400 eV

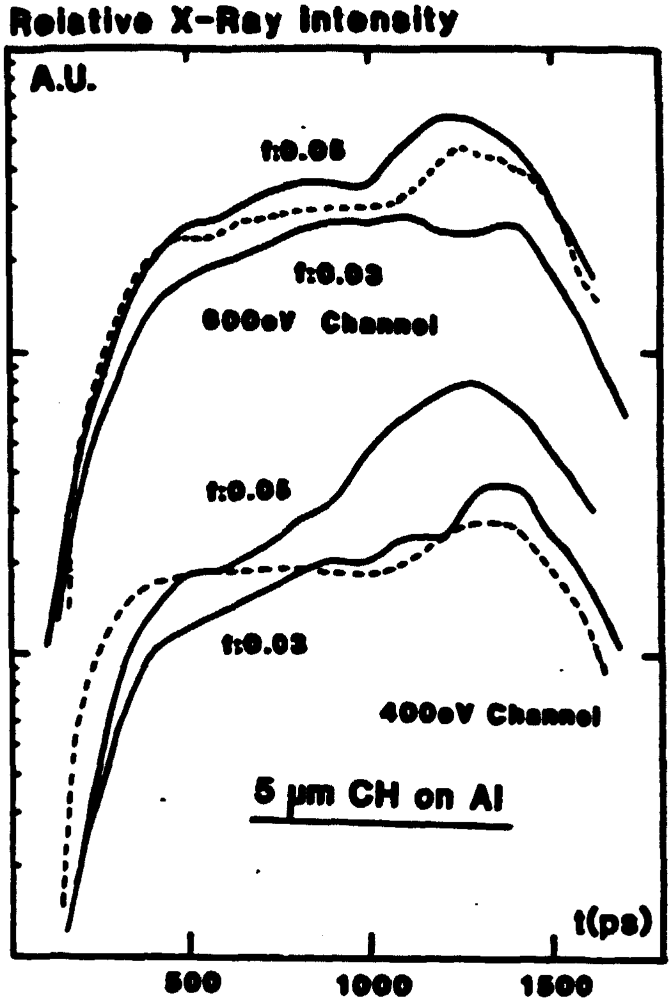

Fig. 8. Calculated and measured X-ray emission time histories ; 5 µm CH coating thickness on aluminum (the curves have arbitrary translated along X-ray intensity axis)

The burnthrough signal corresponds approximately to the crossing of 10^6 K isotherm. On figure 9, we have plotted the measured burnthrough times and compared them to the propagation of 10^6 K isotherm calculated with different flux limiter values ; for f = 0.03 the total ablated polystyrene thickness is 5.8 µm.

In a two dimensional simulation performed with f = 0.03 the thermal front propagation for radius smaller than about 70 µm is almost the same as in 1D calculations, with equivalent flux limiter. The calculated lateral diffusion is weak.

The X-ray images on figure 2 are consistent with a little lateral transport : the emission diameter is independent of plastic coating thickness. But this result is not completely conclusive as we imaged only high temperature regions (Te > 3 10^6 K).

Other diagnostics. The XRD systems gave an estimation of the total radiated X-ray energy. The angular distribution of X-ray emission cannot be determined accurately with only two detectors ; complementary data have been obtained by tilting the target for some shots.

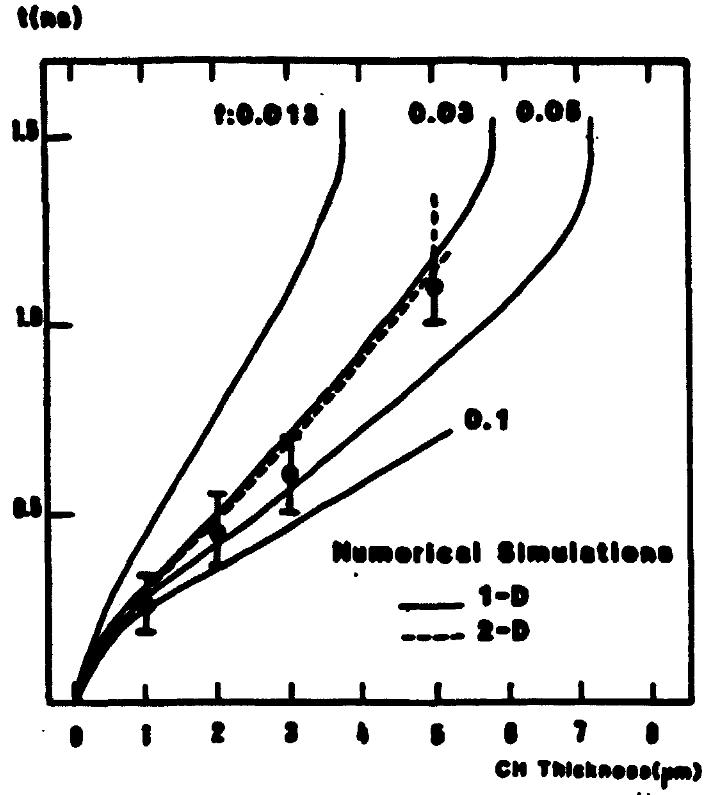

Fig. 9. Measured burnthrough times and calculated ablation front propagation (Te = 10^6 K)

As shown by Mead et al [12], the evaluation of X-ray conversion efficiency as a function of the coating thickness, allows a determination of the flux limiter.

We have followed the same procedure Fig. 10 and the results are quite consistant with those obtained previously i.e. for $f \simeq 0.03$.

A last determination of the ablated mass was given by aluminum line spectroscopy [9]. Fig. 11 shows the relative intensity of the $1s^2 - 1s^2p$ line of Al^{+11} versus polystyrene coating thickness, it indicates an ablated coating thickness of (5.5 ± 0.5) μm. This value corresponds approximately to the plastic depth heated above 3 10^6 K ; it is very close to the result deduced from numerical simulations of time resolved X-ray emission (5.8 μm) with $f \simeq 0.03$.

DISCUSSION

At (6.0 + 2.0) 10^{14} W/cm^2 incident intensity, we have measured an ablated depth of (6.0 ± 0.5) μm, which corresponds to a mass ablation rate $\dot{m} = (8.4 \pm 1)\ 10^5$ g/cm^2.s. The 22°5 beams incidence can be taken into account in 1D simulations by an effective laser wavelength of $0.35 \times \cos^{-1} 22°5 = 0.38$ μm ; if we assume that in scales as $\lambda^{-4/3}$ [24], the ablation rate at normal incidence would have been $(8.4 \pm 1)\ 10^5 \times \cos^{-4/5}(22.5) = (9.3 \pm 1.1)\ 10^5$ g/cm^2.s. This value is in good agreement with other layered plane target experiments [9 10 12], see Fig. 12. Similar results have also been obtained at LLE, with uniformly, illuminated spherical targets (24 beams Omega laser facility) [23]. This agreement between spherical and plane target experiments is rather satisfactory because we have assumed that lateral diffusion was negligible in our experiments ; it might also indicate that the effects on axial transport of the magnetic fields created at the edge of the focal spot are weak.

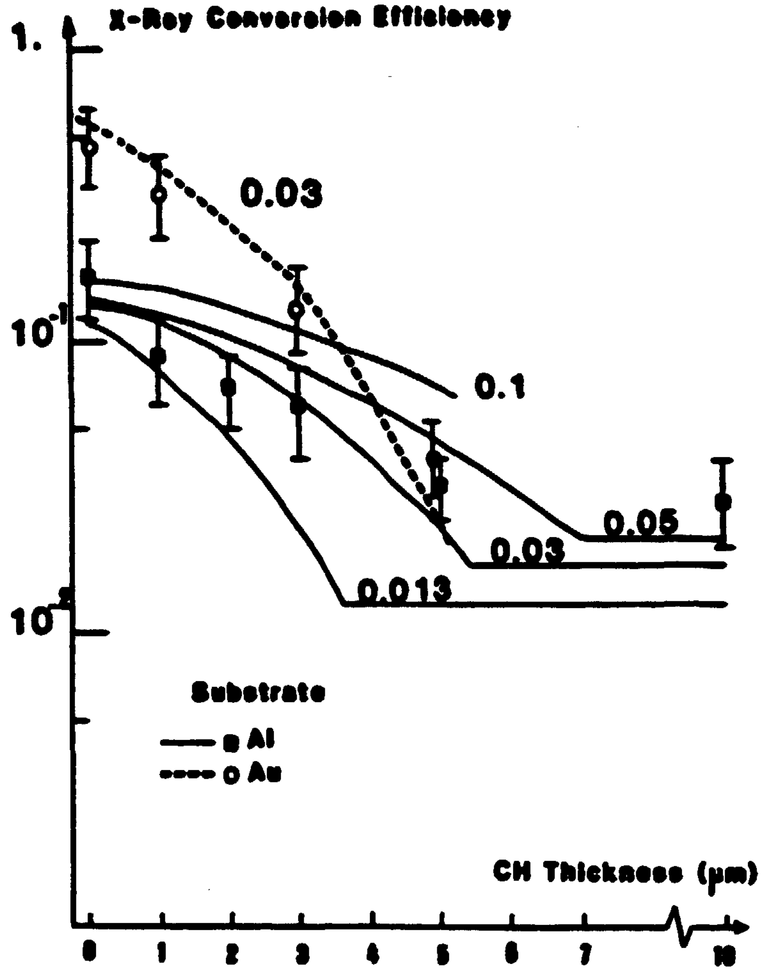

Fig. 10. Measured and calculated total X-ray emission efficiency, for Au and Al substrate, as a function of plastic coating thickness.

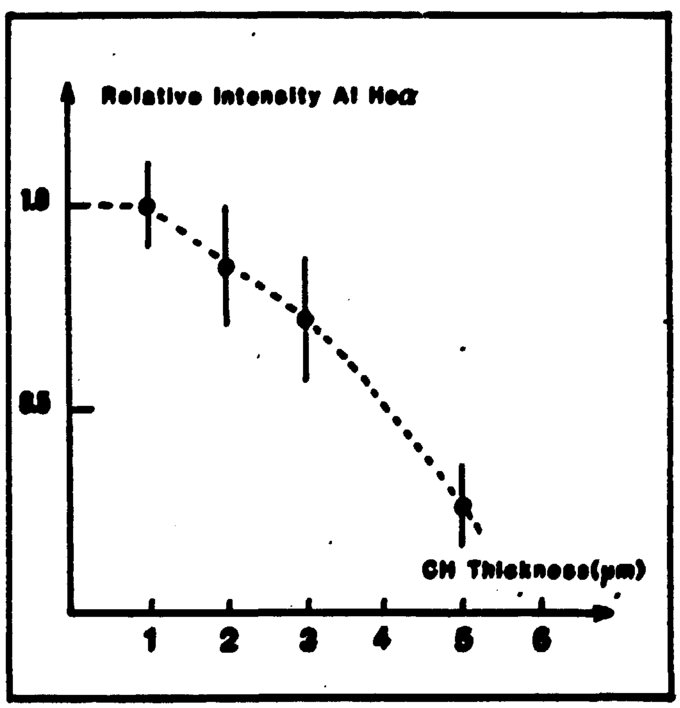

Fig. 11. Relative intensity of Al Heα line as a function of plastic coating thickness.

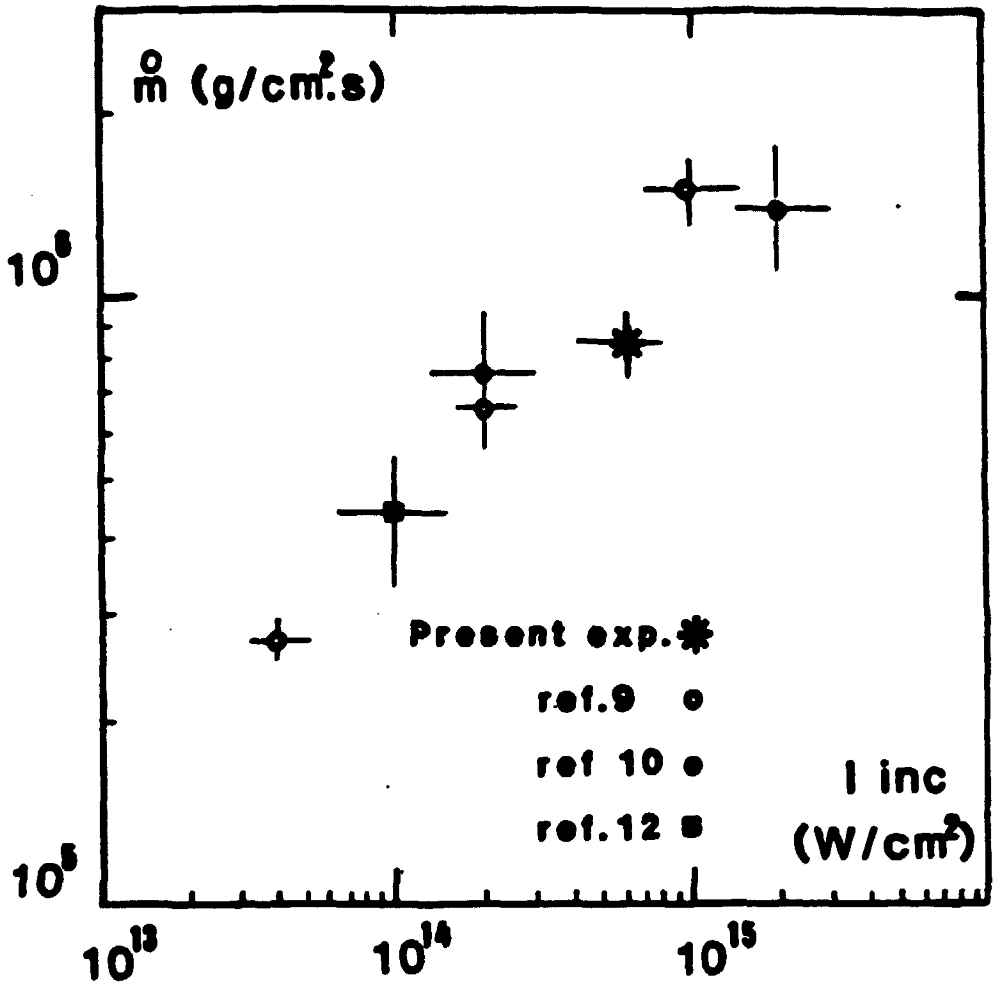

Fig. 12. Summary of measured mass ablation rate per unit area in some plane targets experiments

Regarding the deduced flux limiter value the comparison is not so clear. Our estimation $f = 0.03 \pm 0.015$ is not very different from the result of Yaakobi et al. [9] $f = 0.04 \pm 0.01$; Mead et al [12] have obtained $f = 0.01$, but they used the relation (1) to calculate the heat flux. So plane target experiments give similar results, but the spherical transport experiments, of Barnouin et al [23] are consistant with $f \simeq 0.1$. This difference cannot be satisfactorily explained.

Our results show no evidence of non local transports effects and are in agreement with the steep heat front calculated by the flux limiter technique ; this point has been justified by Holstein et al [7].

The advantage of the experimental method we have employed are quite obvious. The time resolution allows, in principle, a single shot determination of f and the soft X-ray range (200 eV - 1 keV) gives informations on rather low temperature zones ($Te \simeq 10^6$ K).

It can be used with other coating materials, or geometries ; on Fig.13 we present examples of different applications.

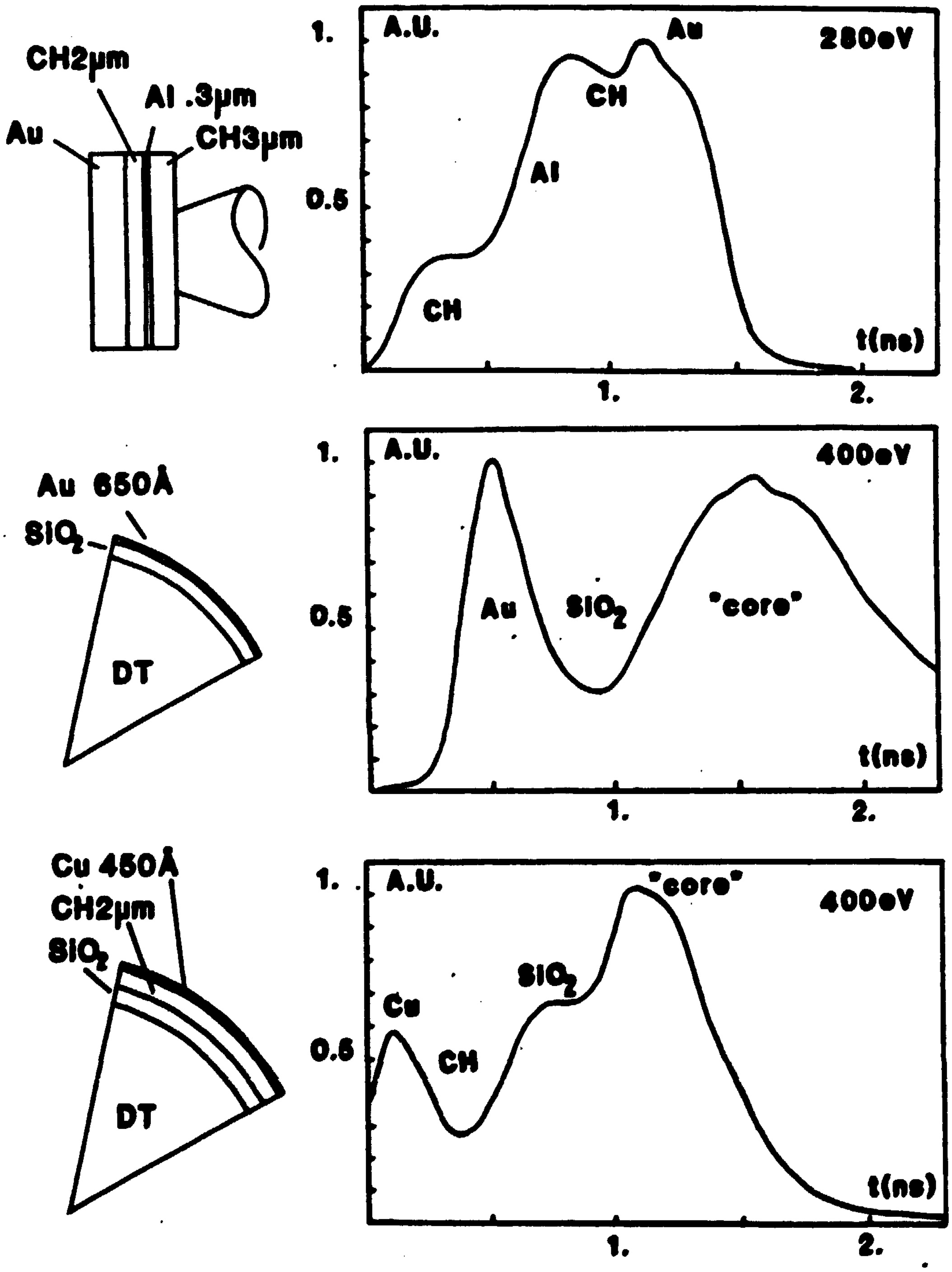

Fig. 13. Examples of transport experiments with time resolved subkiloelectronvolt X-ray emission

CONCLUSION

We have studied the time histories of X-ray emission, in the range 200 eV-1.3 keV, of plane layered targets, irradiated at $\lambda = 0.35\ \mu m$ and $6\ 10^{14}\ W/cm^2$ intensity. This method allows an estimation of heat front velocity and profile ; it was compared to some other ablation rate measurement method. For CH coating we have obtained $\dot{m} = (8.5\pm1) 10^5 g/cm^2 s$, if we neglect lateral transport, 1D simulations with $f = 0.03\pm0.015$ gave account of the main features of our experiments.

ACKNOWLEDGMENTS

The authors appreciate helpfull discussions with M. Busquet, M. Decroisette, A. Decoster, J. Launspach, B. Meyer and F. Thais. They acknowledge the laser team, the target fabrication group and the numerical code development group, especially E. Buresi, C. Leromain and J.N. Richet, for their effective contribution ; they have greatly appreciated the technical assistance of H. Croso, C. Geynes, J. Kobus, J.L. Larcade, G. Lidove, G. Pillon and J. Turberville.

REFERENCES

1. It is not possible to give a review of these experiments, but references can be found in :
   - M.G. Haines, "Laser-Plasma Interactions" 20th Scottish Universities Summer School in Physics, 1979 edited by R.A. Cairns and J.J.Sanderson
   - C.E. Max, "Proceeding of the Les Houches Summer School of Theoretical Physics" edited by R. Balian and J.C. Adam (North-Holland, Amsterdam, 1981) vol. 34
2. C.E. Max, C.F. McKee and W.C. Mead, Phys. Fluids 23, 1620 (1980)
3. W.L. Kruer, Comments Plasma Phys. Controlled Fusion 6, 167 (1981)
4. D.R. Gray and D.J. Kilkenny, Plasma Phys. 22, 81 (1980)
5. L. Spitzer and R. Harm, Phys. Rev. 89, 977 (1953)
6. A.R. Bell, R.G. Evans and D.J. Nicholas, Phys. Rev. Lett. 46, 243 (1981). J.P. Matte and J. Virmont, Phys. Rev. Lett. 49, 1936 (1982). A.R. Bell, Phys. Fluids 28, 6, 2007 (1985)
7. J.F. Luciani, P. Mora and R. Pellat, Phys. Fluids 28, 835 (1985) P.A. Holstein et al. 15th Anomalous Absorption Conference, Banff, June 1985
8. F.C. Young et al, Appl. Phys. Lett. 30, 45 (1977)
9. B. Yaakobi et al, Optics Comm. 39, 175 (1981)
10. M.H. Key et al, Phys. Fluids, 26, 7, 2011 (1983)
11. M.C. Richardson et al., IEEE Journal of Quant. Electron., Q.E. 19, 1861 (1983)
12. W.C. Mead et al, Phys. Fluids 27, 5, 1301 (1984)
13. G.L. Stradling, Ph. D. Thesis UCRL 53271 (1982)
14. J. Launspach et al, SPIE, 491, High Speed Photography (Strasbourg 1984), 685
15. C. Cavailler, N. Fleurot, J. Launspach, R. Sauneuf, R. Verrecchia SPIE, 348, High Speed Photography (San Diego 1982), 760
16. R.L. Keck, L.M. Goldman, M.C. Richardson, W. Seka, K. Tanaka Phys. Fluids, 27, 11, 2762 (1984)
17. W. Seka et al, Optics Comm. 40, 6, 437 (1982)
18. M.C. Richardson et al, Phys. Rev. Lett. 54, 15, 1656 (1985)
19. M. Busquet, Phys. Rev. A 25, 4, 2302, (1982)
    M. Busquet, 5th Topical Conf. on Atomic Processes in High Temperature Plasmas, Pacific Grove, Feb. 1985
20. J.M. Dawson, P. Kaw and B. Green, Phys. Fluids 12, 875 (1968)
21. W. Seka et al, Optics Comm. 40, 6, 437 (1982)
22. M.C. Richardson et al, Phys. Rev. Lett., 54, 15, 1656 (1985)

23. O. Barnouin et al, 15th Anomalous Absorption Conference, Banff, june 1985
24. B. Meyer and G. Thiell, Phys. Fluids, 27, 1, 302 (1985)